NASA Technical Memorandum 105415

Fast Methods to Numerically Integrate the Reynolds Equation for Gas Fluid Films

Florin Dimofte
Lewis Research Center
Cleveland, Ohio

Prepared for the
STLE–ASME Joint Tribology Conference
St. Louis, Missouri, October 13–16, 1991

FAST METHODS TO NUMERICALLY INTEGRATE THE REYNOLDS EQUATION FOR GAS FLUID FILMS

Florin Dimofte*
National Aeronautics and Space Administration
Lewis Research Center
Cleveland, Ohio 44135

SUMMARY

The alternating direction implicit (ADI) method is adopted, modified, and applied to the Reynolds equation for thin, gas fluid films. An efficient code is developed to predict both the steady-state and dynamic performance of an aerodynamic journal bearing. An alternative approach is shown for hybrid journal gas bearings by using Liebmann's iterative solution (LIS) for elliptic, partial differential equations.

The results are compared with known design criteria from experimental data. The developed methods show good accuracy and very short computer running time in comparison with methods based on an inverting of a matrix. The computer codes need a small amount of memory and can be run on either personal computers or on mainframe systems.

INTRODUCTION

The Reynolds partial differential pressure equation for a compressible, thin, fluid film is nonlinear and involves a great deal of numerical effort to solve. From the early sixties to the present time several methods were developed for numerically solving this equation. Major contributions were made by Castelli and Pirvics, Booy, Coleman, Castelli in Gross' book, and others (refs. 1 to 4). The columnwise influence coefficients method introduced by Castelli was one of the best at that time. The present work is focused basically on two methods (alternating direction implicit method (ADI) and Liebmann's iterative solution (LIS)), which add important advantages to the numerical solution technique of the compressible Reynolds equation.

The Reynolds equation in dimensionless form for a compressible-fluid-film journal bearing subject to isothermal conditions is (ref. 5)

$$\frac{\partial}{\partial\theta}\left(h^3\frac{\partial p^2}{\partial\theta}\right)+\frac{\partial}{\partial z}\left(h^3\frac{\partial p^2}{\partial z}\right)=2\Lambda\frac{\partial(ph)}{\partial\theta}+2\Lambda_z\frac{\partial(ph)}{\partial z}+i4f\Lambda\frac{\partial(ph)}{\partial\tau} \tag{1}$$

Both steady-state and dynamic analyses to calculate the static and dynamic performance of an aerodynamic journal bearing are shown in the appendix A. Starting from equation (1), the following partial differential equation are developed in appendix A:

---

*National Research Council-NASA Research Associate at Lewis Research Center.

$$\frac{\partial^2 Q_0}{\partial \theta^2} + \frac{\partial^2 Q_0}{\partial z^2} - \frac{1}{h_0}\left(\frac{\partial h_0}{\partial \theta} + \frac{\Lambda}{\sqrt{Q_0}}\right)\frac{\partial Q_0}{\partial \theta} - \frac{1}{h_0}\left(\frac{\partial h_0}{\partial z} + \frac{\Lambda_z}{\sqrt{Q_0}}\right)\frac{\partial Q_0}{\partial z} - \frac{2}{h_0}\left(\frac{\partial^2 h_0}{\partial \theta^2} + \frac{\partial^2 h_0}{\partial z^2}\right) Q_0 = 0 \tag{2}$$

$$\frac{\partial^2 Q_1}{\partial \theta^2} + \frac{\partial^2 Q_1}{\partial z^2} - \frac{1}{h_0}\left(\frac{\partial h_0}{\partial \theta} + \frac{\Lambda}{\sqrt{Q_0}}\right)\frac{\partial Q_1}{\partial \theta} - \frac{1}{h_0}\left(\frac{\partial h_0}{\partial z} + \frac{\Lambda_z}{\sqrt{Q_0}}\right)\frac{\partial Q_1}{\partial z} - \frac{1}{h_0}\left(2\frac{\partial^2 h_0}{\partial \theta^2} - \frac{\Lambda}{2{Q_0}^{3/2}}\frac{\partial Q_0}{\partial \theta}\right.$$

$$\left. + 2\frac{\partial^2 h_0}{\partial z^2} - \frac{\Lambda_z}{2{Q_0}^{2/3}}\frac{\partial Q_0}{\partial z} + i\,\frac{2f\Lambda}{\sqrt{Q_0}}\right) Q_1 = -\frac{1}{2h_0}\left(\frac{\partial^2 Q_0}{\partial \theta^2}\cos\theta + \frac{\partial Q_0}{\partial \theta}\sin\theta + 2Q_0\cos\theta + \frac{\partial^2 Q_0}{\partial z^2}\cos\theta\right) \tag{3}$$

$$\frac{\partial^2 Q_2}{\partial \theta^2} + \frac{\partial^2 Q_2}{\partial z^2} - \frac{1}{h_0}\left(\frac{\partial h_0}{\partial \theta} + \frac{\Lambda}{\sqrt{Q_0}}\right)\frac{\partial Q_2}{\partial \theta} - \frac{1}{h_0}\left(\frac{\partial h_0}{\partial z} + \frac{\Lambda_z}{\sqrt{Q_0}}\right)\frac{\partial Q_2}{\partial z} - \frac{1}{h_0}\left(2\frac{\partial^2 h_0}{\partial \theta^2} - \frac{\Lambda}{2{Q_0}^{3/2}}\frac{\partial Q_0}{\partial \theta}\right.$$

$$\left. + 2\frac{\partial^2 h_0}{\partial z^2} - \frac{\Lambda_z}{2{Q_0}^{2/3}}\frac{\partial Q_0}{\partial z} + i\,\frac{2f\Lambda}{\sqrt{Q_0}}\right) Q_2 = -\frac{1}{h_0}\left(\frac{\partial^2 Q_0}{\partial \theta^2}\sin\theta - \frac{\partial Q_0}{\partial \theta}\cos\theta + 2Q_0\sin\theta + \frac{\partial^2 Q_0}{\partial z^2}\sin\theta\right) \tag{4}$$

Equation (2) is used to perform the steady-state characteristics; while equations (3) and (4) are used to compute the dynamic performance. The numerical integration techniques for these equations are developed and discussed in herein.

SYMBOLS

a_{ij}, b_{ij}, c_{ij},

d_{ij}, e_{ij}, r_{ij} coefficients of grid node eq. (6)

a supply orifice radius, m

B_c symbolic damping coefficient used in stability analysis (see eq. (A-27))

B_{ij} dynamic damping coefficient, $N{\cdot}m^{-1}{\cdot}s^{-1}$

C journal bearing radial clearance, m

C_D orifice supply discharge coefficient

D journal bearing diameter, m

d orifice supply hole diameter, m

e	eccentricity (see fig. 1), m
e_{max}	maximum iteration step error (see eq. (12))
F	load capacity (the resulting force of the pressure distribution), N
F	$F/(p_a LD)$ dimensionless load capacity (eq. (18))
F_r, F_t	component of F along and perpendicular to the centerline, respectively (see fig. 1)
F_{r0}, F_{t0}	steady-state component of F
F_x, F_y	dynamic component of F along x and y directions (see fig. 1)
f	whirl frequency ratio, ν/Ω
f_0	unstable whirl frequency ratio, ν_0/Ω
G_m	dimensionless supply flow part that is function of p_m/p_s (see eq. (B-11))
h	dimensionless film thickness, $\overline{h}/C$
$\overline{h}$	film thickness, m
h_0	steady-state component of h
h_m	film thickness at the supply orifice (see fig. 13)
i	$-1^{1/2}$ the imaginary unit
i_i	the unit vector along x_i direction (see fig. 14)
K	stiffness, $N \cdot m^{-1}$
K	dimensionless stiffness (see eq. (21))
K_{ij}	dynamic stiffness coefficient
K_c, K_{c0}	symbolic stiffness coefficient used in stability analysis (see eqs. (A-27) and (A-29))
L	bearing length, m
l	length vector part of the C_m boundary of integral (B-7) (see also fig. 14)
M	rotor mass allocated to one bearing; for a symmetric rotor M is half of the rotor mass, kg
M_c	corresponding rotor mass, allocated to one bearing, required to make the bearing unstable, kg
M,N	number of grid points in i and j directions

n	unit vector outward, perpendicular to the C_m boundary (see n_{ij} in fig. 14)
n_0	total number of supply orifices
$\overline{p}$	pressure, Pa
p	dimensionless pressure
$\overline{p}_a$	ambient pressure, Pa
p_{1a}, p_{2a}	boundary pressure at bearing edges
p_m	pressure downstream of the supply system
p_0	steady-state component of the pressure p (see eq. (A-6))
p_s	supply pressure, Pa
p_1, p_2	perturbation components of pressure p (see eq. (A-6))
Q	dimensionless pressure variable, $(ph)^2$
Q_0, Q_1, Q_2	steady-state and perturbation components of Q (see eq. (A-7))
q_m	dimensionless flow through the pocketed orifice supply restrictor system
R	journal bearing radius, m
ρ	gas constant (see eq. (B-9)), $J \cdot kg^{-1} \cdot K^{-1}$
r, t	coordinates (fig. 1)
S_T	threshold speed, $\Omega(M_c\ C/W)^{1/2}$
T	absolute temperature (see eq. (B-9)), K
t	time, s
V_z	axial velocity (shaft speed along z direction), $m \cdot s^{-1}$
W	bearing load, N
x, y	whirl amplitude of the journal center in bearing (see eqs. (A-20) and (A-25))
$x_{1,3}$	fluid film coordinates (see eq. (A-1) and fig. 14)
Z_{ij}	impedance for translatory motion
z	axial coordinate parallel to rotor axis

γ	adiabatic exponent
Δz	increment in z direction
$\Delta\theta$	increment in θ direction
δ	pocketed orifice compensation factor, a^2/dC
ϵ	eccentricity ratio, e/R
ϵ_0	eccentricity ratio under static load
$\epsilon_0\phi_1$	dimensionless tangential whirl amplitude
ϵ_1	dimensionless radial whirl amplitude
θ	angular coordinate from centerline (see fig. 1)
Λ	bearing number (see eq. (A-2) and (B-5))
Λ_z	equivalent bearing number in z direction (see eq. (A-2))
Λ_s	restrictor coefficient (see eq. (B-9))
λ	relaxation coefficient (see eq. (10))
μ	dynamic viscosity, $N{\cdot}s{\cdot}m^{-2}$
ν	whirl frequency, $rad{\cdot}s^{-1}$
ν_0	unstable whirl frequency
τ	dimensionless time (see eq. (A-1))
ϕ	attitude angle, deg
ϕ_0	attitude angle under static load, deg
Ω	rotation frequency, $rad{\cdot}s^{-1}$
Ω_1	shaft rotation frequency, $rad{\cdot}s^{-1}$
Ω_2	bearing housing rotation frequency, $rad{\cdot}s^{-1}$

Subscripts:

i,j	grid index
r	centerline direction (see fig. 1)

t perpendicular to center-line direction (see fig. 1)

x x-direction (direction of the static load on bearing, see fig. 1)

y y-direction perpendicular to x (see fig. 1)

Superscripts:

n old iteration step

$n + 1$ new iteration step

$(n + 1)/2$ half step iteration between n and $n + 1$

NUMERICAL COMPUTATION

In order to integrate equations (2) to (4), a finite-difference numerical method is adopted. This method can handle a plain, cylindrical, journal bearing of finite length (fig. 1) with a high degree of accuracy. Using a rectangular grid with constant spacing between nodes in both directions, the partial derivatives become

$$\left(\frac{\partial Q}{\partial \theta}\right)_{i,j} = \frac{Q_{i,j+1} - Q_{i,j-1}}{2\Delta\theta} \tag{5}$$

$$\left(\frac{\partial Q}{\partial z}\right)_{i,j} = \frac{Q_{i+1,j} - Q_{i-1,j}}{2\Delta z} \tag{6}$$

$$\left(\frac{\partial^2 Q}{\partial \theta^2}\right)_{i,j} = \frac{Q_{i,j+1} - 2Q_{i,j} + Q_{i,j-1}}{(\Delta\theta)^2} \tag{7}$$

$$\left(\frac{\partial^2 Q}{\partial z^2}\right)_{i,j} = \frac{Q_{i+1,j} - 2Q_{i,j} + Q_{i-1,j}}{(\Delta z)^2} \tag{8}$$

where

$$\Delta\theta,\ \Delta z = \text{node spacing} \tag{9}$$

At node (i,j) of the grid, equation (2) has the general form

$$a_{i,j}Q_{0_{i-1,j}} + b_{i,j}Q_{0_{i+1,j}} + c_{i,j}Q_{0_{i,j-1}} + d_{i,j}Q_{0_{i,j+1}} + e_{i,j}Q_{0_{i,j}} = r_{i,j} \tag{10}$$

Thus, a linear system of M × N equations results if the grid has M and N points in the z and θ directions, respectively. Unfortunately, the coefficients of equation (10) depend on the value of the variable Q so that an iterative method has to be used to compute the steady-state component of Q.

First, the system of equations (10) must be solved. Then, since

$$Q_0 \rightarrow p_0 \tag{11}$$

and all the steady-state characteristics, the equations (3) and (4) can be solved, using the same finite difference method, to calculate the dynamic performance.

ALTERNATING DIRECTION IMPLICIT SCHEME

The linear system (10) can be efficiently solved using the alternating direction implicit (ADI) scheme (ref. 6), which changes the linear system of equation (10) into a tri-diagonal linear system using a proper iterative manner. The tri-diagonal system can be solved with Thomas' algorithm. In order to use the ADI method, equation (10) was written as follows for the first and second half step of the iteration n + 1:

$$a_{i,j}\,(Q_{i-1,j})^{(n+1)/2} + e_{i,j}\,(Q_{i,j})^{(n+1)/2} + b_{i,j}\,(Q_{i+1,j})^{(n+1)/2} = r_{i,j} - c_{i,j}\,(Q_{i,j-1})^{n} - d_{i,j}\,(Q_{i,j+1})^{n} \tag{12}$$

and then

$$c_{i,j}\,(Q_{i,j-1})^{n+1} + e_{i,j}\,(Q_{i,j})^{n+1} + d_{i,j}\,(Q_{i,j+1})^{n+1} = r_{i,j} - a_{i,j}\,(Q_{i-1,j})^{(n+1)/2} - b_{i,j}\,(Q_{i+1,j})^{(n+1)/2} \tag{13}$$

This same scheme was applied to equations (3) and (4) to obtain the dynamic characteristics.

Using the ADI method, the computer running time for one case (one eccentricity ratio) is reduced from 1 hr to 1 to 5 min (using a 20×9 grid and a 386, 20-MHz personal computer). To decrease the total time to reach solution convergence, equation (11) can be used alone.

The convergence is difficult for equation (2), (3), or (4) for bearing numbers (eq. (A-2)) greater than 10. Also, the convergence of the numerical solution is sometimes difficult when the stability of the bearing is analyzed, especially at high bearing numbers. One possibility to improve the convergence is to use a relaxation technique:

$$Q^{n+1} \rightarrow \lambda Q^{n+1} + (\,1 - \lambda)\,Q^{n} \tag{14}$$

where

$$\lambda = 0 \rightarrow 1$$

A second possibility is to convert the dimensions of the grid from a large one (e.g., from $N \times M = 40 \times 33$ or 30×25 or 20×17), used to compute the steady-state component Q_0 of the variable Q (eq. (A-7)) and the derivatives of Q_0 and h_0, to a small one (e.g., 10×9) and then to compute the dynamic components Q_1 and Q_2 of the variable Q.

LIEBMANN'S ITERATIVE SOLUTION

The discretization of the Reynolds equation results in a large linear system of equations that needs to be solved. For example, a 20 by 9 grid involves 180 linear algebraic equations like equation (10). There are a maximum of five unknown terms per line in equation (10). For a large-sized grid, many of the terms will be zero. For such a sparse system, the elimination methods waste significant computer memory to store zeros. To avoid these difficulties, the LIS method (ref. 7) can be used as an alternative to ADI. In this technique equation (10) is expressed as

$$Q_{i,j} = \frac{R_{i,j} - A_{i,j}\, Q_{i-1,j} - B_{i,j}\, Q_{i+1,j} - C_{i,j}\, Q_{i,j-1} - D_{i,j}\, Q_{i,j+1}}{E_{i,j}} \tag{15}$$

and solved iteratively for $j = 1$ to N and $i = 1$ to M. Because equation (10) is diagonally dominant for most of the bearing running conditions, this procedure will eventually converge to a stable solution. Note that the coefficients C, D, and E depend on the value of the variable Q from the previous iteration. As with the ADI method, a relaxation technique can be used to improve the convergence of this method. The relaxation coefficient, λ, can be variable and under control of the maximum error for each iteration step calculated as

$$\epsilon_{max} = \text{Max} \left| \frac{(Q_{i,j})^{n+1} - (Q_{i,j})^{n}}{(Q_{i,j})^{n+1}} \right| \tag{16}$$

for

$$i = 1 \rightarrow M\,, \quad j = 1 \rightarrow N \tag{17}$$

One of the most difficult cases regarding the convergence is the hybrid, compressible-fluid, film bearing. This case balances the flow through the supply restriction system with the flow through the fluid film to calculate the downstream pressure in the supply port. This requires an additional iteration loop. Also, the equation of the flow through a restriction system, like a pocketed orifice, is a combination of four relations that is a function of the type of flow (choked or unchoked) and the direction of the flow (in or out). The analysis of a hybrid, compressible fluid bearing is outlined in appendix B.

RESULTS AND DISCUSSION

ADI Method

Both steady-state and dynamic performance results over a range of bearing number Λ (A-3) from 0.903 to 9.03 and an eccentricity ratio between 0.1 and 0.6 are very close to known computed data from (refs. 8 and 9). Figures 2 and 3 show the basic steady-state characteristics: load capacity and attitude angle (fig. 1 and eq. (A-19)) versus bearing number. The dimensionless form of the load capacity is

$$F = \frac{\bar{F}}{p_a LD} \tag{18}$$

The numerically computed steady-state data using the ADI method agree well with Raimondi data (ref. 8) for both grid dimensions used (20×9 and 10×5). The same conclusion arises in figures 4 and 5 where the whirl frequency ratio and threshold speed criteria are shown. The whirl frequency ratio is

$$f_0 = \frac{\nu_0}{\Omega} \tag{19}$$

and the threshold speed is

$$S_T = \frac{\Omega}{\sqrt{p_a LD}} \sqrt{\frac{M_c C}{\frac{W}{p_a LD}}} = \Omega \sqrt{\frac{M_c C}{W}} \tag{20}$$

The notation used in equations (19) and (20) are described in appendix A. In figures 4 and 5 the ADI computed data are compared with Chang and Pan's computed data (ref. 9). An exception to this general conclusion may be for the threshold speed at low bearing numbers and especially at small eccentricity ratios (left bottom corner of fig. 5) where the ADI computed data show more sensitive behavior to the "half frequency instability" than the data from Chang and Pan. No experimental data were found for this particular range of input data.

LIS Method

The LIS method is first used to compute the steady-state performance of an aerodynamic journal bearing. To assess the accuracy of the LIS method, both LIS and Raimondi data are shown in figure 6 for load capacity and in figure 7 for attitude angle. Very good agreement was obtained for a range of the bearing numbers between 0.1 and 17. The grid has 30×9, 40×9, and 60×9 nodes, and the computing time for one case (one point in either fig. 6 or 7) is regularly less than 1 min.

The LIS hybrid gas bearing code was first used to compute the steady-state characteristics of a double-plane supply aerostatic journal bearing with a length to diameter ratio L/D of 2. The output data for the dimensionless stiffness as was defined in (ref. 10) as

$$K = \frac{1 + \delta^2}{1 + \frac{2}{3}\delta^2} \frac{C\,K}{(p_s - p_a)\,LD} \tag{21}$$

versus restrictor coefficient (eq. (B-9)) was plotted in figure 8. The notation used in equation (21) is shown in appendix B. Based on an average stiffness calculation, the eccentricity of the shaft was 0.05, 0.1, and 0.5 of the radial clearance (curves LIS 0.05, 0.1, and 0.5 respectively). For comparison, the corresponding curve from Wilcock (ref. 10) and Pink's experimental data (ref. 11) are also plotted in figure 8. Pink's data (ref. 11) were obtained using the stiffness near zero eccentricity and the load at 0.5 eccentricity. The LIS computed data agree well with Pink's experimental data.

The computed total load and stiffness for a hybrid journal gas bearing is shown in figures 9 and 10. Both externally pressurized and dynamic effects contribute to pressure rises in the fluid film. The dynamic effects contribute a significant amount to the total load, especially at high eccentricity ratios and high speeds. Figure 10 and especially figure 11 indicate that, for small eccentricity ratios (near zero), the dynamic effects can diminish the bearing performance in turning the shaft at low speeds. The radial flow due to the rotation of the shaft appears to change the externally supplied flow. This change results in the load and stiffness of the hybrid bearing (turning speeds of 5000 and 15000 rpm) being lower than the aerostatic bearing curve (0 rpm) for eccentricity ratios 0 to 0.2. This phenomenon is controlled by the turning speed and by the radial clearance ratio. Figure 11 shows how radial clearance affects the bearing stiffness for turning speeds of 0 and 5000 rpm.

CONCLUSIONS

Two methods (alternating direction implicit (ADI) and Ziebmann's iterative solution (LIS)) were adopted and modified to integrate the compressible pressure-differential equation. The ADI method was used to compute the steady-state and the dynamic performance of an aerodynamic journal bearing. Both steady-state and dynamic results are in good agreement with known design criteria. The LIS method was used to calculate the pressure distribution of a hybrid journal gas bearing. Because a hybrid bearing needs an additional iteration loop to balance the flow through the supply system with the flow through the lubrication film, convergence takes longer. Both numerical methods (ADI and LIS) are more efficient, in terms of running time of the codes, than other known methods. However, the ADI method sometime shows poor convergence, especially for dynamic computation at very low or very high bearing numbers. The LIS method can handle the aerodynamic, the aerostatic, and the hybrid bearings and can generate useful data, especially for hybrid gas bearings. Furthermore, the LIS method can provide data with minimal computer time. Both methods (ADI and LIS) provide data with running computing times between 10 to 50 times faster than other methods that involve inverting a matrix. The running time for the ADI or LIS method is proportional to the grid dimension.

ACKNOWLEDGMENTS

This paper arises from the work done at the NASA Lewis Research Center, Cleveland, Ohio, in a NRC Associateship Program. I would like to thank Jim Walker, Gene Addy, and David Brewe from NASA Lewis who kindly reviewed this paper and D. Vijayaraghavan for his suggestions concerning the ADI method.

APPENDIX A. — STEADY-STATE AND DYNAMIC ANALYSES OF A PLAIN, CYLINDRICAL, FINITE LENGTH, SELF-ACTING GAS JOURNAL BEARING.

The Reynolds equation in dimensionless form for a compressible-fluid-film journal bearing subject to isothermal conditions is (refs. 4 and 5)

$$\frac{\partial}{\partial\theta}\left(h^3\frac{\partial p^2}{\partial\theta}\right)+\frac{\partial}{\partial z}\left(h^3\frac{\partial p^2}{\partial z}\right)=2\Lambda\frac{\partial(ph)}{\partial\theta}+2\Lambda_z\frac{\partial(ph)}{\partial z}+i4f\Lambda\frac{\partial(ph)}{\partial\tau} \tag{1}$$

where

$$p=\frac{\bar{p}}{p_a},\ \theta=\frac{x_1}{R},\ z=\frac{x_3}{R}\ \tau=i\ \nu t,\ \left(i=\sqrt{-1}\right) \tag{A-1}$$

$$\Lambda=\frac{6\mu(\Omega_1+\Omega_2)}{p_a}\left(\frac{R}{C}\right)^2,\quad \Lambda_z=\frac{6\mu}{p_a}\frac{V_z}{R}\left(\frac{R}{C}\right)^2 \tag{A-2}$$

$$f=\frac{\nu}{\Omega}\ (\Omega=\Omega_1+\Omega_2) \tag{A-3}$$

and where Ω_1 is the shaft rotating speed, Ω_2 is the bearing rotating speed, ν is the whirl frequency (in radians per second), ν_z is the shaft axial speed, and μ is the dynamic viscosity.

Both circumferential and axial movement are taken into account in equation (A-1), and a complex form for time-dependent terms is used for the dynamic analyses.

In order to integrate equation (1), a natural linearization procedure is applied (ref. 1) by writing Reynolds equation in terms of a new variable $Q=(ph)^2$. For the dynamic analyses, a small perturbation technique was used. Here, the journal center was assigned a static eccentricity ratio ϵ_0 and a corresponding attitude angle ϕ_0. This position was perturbed by a small amplitude harmonic motion:

$$\epsilon=\epsilon_0+\epsilon_1 e^{\tau},\ \varphi=\varphi_0+\varphi_1 e^{\tau} \tag{A-4}$$

The corresponding perturbed forms of the dimensionless film thickness and pressure can be written as

$$h=h_0+\epsilon_1 e^{\tau}\cos\theta+\epsilon_0\varphi_1 e^{\tau}\sin\theta \tag{A-5}$$

$$p=p_0+\epsilon_1 e^{\tau}\,p_1+\epsilon_0\varphi_1 e^{\tau}\,p_2 \tag{A-6}$$

Introducing a new variable

$$Q = (ph)^2 = Q_0 + 2\,\epsilon_1 e^{\tau}\,Q_1 + 2\,\epsilon_0\varphi_1 e^{\tau}\,Q_2 \tag{A-7}$$

and substituting equations (A-5), (A-6), and (A-7) into equation (1) yield

$$\frac{\partial^2 Q_0}{\partial\theta^2} + \frac{\partial^2 Q_0}{\partial z^2} - \frac{1}{h_0}\left(\frac{\partial h_0}{\partial\theta} + \frac{\Lambda}{\sqrt{Q_0}}\right)\frac{\partial Q_0}{\partial\theta} - \frac{1}{h_0}\left(\frac{\partial h_0}{\partial z} + \frac{\Lambda_z}{\sqrt{Q_0}}\right)\frac{\partial Q_0}{\partial z} - \frac{2}{h_0}\left(\frac{\partial^2 h_0}{\partial\theta^2} + \frac{\partial^2 h_0}{\partial z^2}\right) Q_0 = 0 \tag{2}$$

$$\frac{\partial^2 Q_1}{\partial\theta^2} + \frac{\partial^2 Q_1}{\partial z^2} - \frac{1}{h_0}\left(\frac{\partial h_0}{\partial\theta} + \frac{\Lambda}{\sqrt{Q_0}}\right)\frac{\partial Q_1}{\partial\theta} - \frac{1}{h_0}\left(\frac{\partial h_0}{\partial z} + \frac{\Lambda_z}{\sqrt{Q_0}}\right)\frac{\partial Q_1}{\partial z} - \frac{1}{h_0}\left(2\frac{\partial^2 h_0}{\partial\theta^2} - \frac{\Lambda}{2{Q_0}^{3/2}}\frac{\partial Q_0}{\partial\theta}\right.$$

$$\left. + 2\frac{\partial^2 h_0}{\partial z^2} - \frac{\Lambda_z}{2{Q_0}^{2/3}}\frac{\partial Q_0}{\partial z} + i\,\frac{2f\Lambda}{\sqrt{Q_0}}\right) Q_1 = -\frac{1}{2h_0}\left(\frac{\partial^2 Q_0}{\partial\theta^2}\cos\theta + \frac{\partial Q_0}{\partial\theta}\sin\theta + 2Q_0\cos\theta + \frac{\partial^2 Q_0}{\partial z^2}\cos\theta\right) \tag{3}$$

$$\frac{\partial^2 Q_2}{\partial\theta^2} + \frac{\partial^2 Q_2}{\partial z^2} - \frac{1}{h_0}\left(\frac{\partial h_0}{\partial\theta} + \frac{\Lambda}{\sqrt{Q_0}}\right)\frac{\partial Q_2}{\partial\theta} - \frac{1}{h_0}\left(\frac{\partial h_0}{\partial z} + \frac{\Lambda_z}{\sqrt{Q_0}}\right)\frac{\partial Q_2}{\partial z} - \frac{1}{h_0}\left(2\frac{\partial^2 h_0}{\partial\theta^2} - \frac{\Lambda}{2{Q_0}^{3/2}}\frac{\partial Q_0}{\partial\theta}\right.$$

$$\left. + 2\frac{\partial^2 h_0}{\partial z^2} - \frac{\Lambda_z}{2{Q_0}^{2/3}}\frac{\partial Q_0}{\partial z} + i\,\frac{2f\Lambda}{\sqrt{Q_0}}\right) Q_2 = -\frac{1}{h_0}\left(\frac{\partial^2 Q_0}{\partial\theta^2}\sin\theta - \frac{\partial Q_0}{\partial\theta}\cos\theta + 2Q_0\sin\theta + \frac{\partial^2 Q_0}{\partial z^2}\sin\theta\right) \tag{4}$$

The equation (2) is the conventional steady-state equation. It is nonlinear and was solved in finite-difference form by an iterative method. The last two equations depend on the steady-state solution. They are linear equations with complex dependent variables and were solved numerically.

Taking into account equations (A-5), (A-6), and (A-7) the following relations can be established:

$$\begin{aligned} Q_0 &= {p_0}^2{h_0}^2 \\ Q_1 &= {p_0}^2 h_0 \cos\theta + p_0{h_0}^2 p_1 \\ Q_2 &= {p_0}^2 h_0 \sin\theta + p_0{h_0}^2 p_2 \end{aligned} \tag{A-8}$$

or

$$p_0 = \frac{\sqrt{Q_0}}{h_0}$$

$$p_1 = \left(\frac{Q_1}{\sqrt{Q_0}} - \frac{\sqrt{Q_0}}{h_0} \cos\theta \right) \frac{1}{h_0} \tag{A-9}$$

$$p_2 = \left(\frac{Q_2}{\sqrt{Q_0}} - \frac{\sqrt{Q_0}}{h_0} \sin\theta \right) \frac{1}{h_0}$$

respectively. The boundary conditions are

$$\begin{aligned} & p_0 = p_{1a}, \quad Q_0 = p_{1a}^2 h_0^2 \\ z = 0, \quad & p_1 = 0, \quad Q_1 = p_{1a}^2 h_0 \cos\theta \\ & p_2 = 0, \quad Q_2 = p_{1a}^2 h_0 \sin\theta \end{aligned} \tag{A-10}$$

$$\begin{aligned} & p_0 = p_{2a}, \quad Q_0 = p_{2a}^2 h_0^2 \\ z = \frac{L}{B}, \quad & p_1 = 0, \quad Q_1 = p_{2a}^2 h_0 \cos\theta \\ & p_2 = 0, \quad Q_2 = p_{2a}^2 h_0 \sin\theta \end{aligned}$$

For a journal bearing a periodic condition is also necessary:

$$p_{\theta=0} = p_{\theta=2\pi} \tag{A-11}$$

The resulting hydrodynamic force will be computed by integration of the film pressure. The force will have a radial component in the opposite direction of the eccentricity (on the centerline) and a tangential component in the direction of the attitude angle under static load:

$$\left.\begin{matrix} F_r \\ F_t \end{matrix}\right\} = p_a R^2 \int_0^{\frac{L}{R}} \int_0^{2\pi} (p_0 - 1 + p_1 \epsilon_1 e^{\tau} + p_2 \epsilon_0 \varphi_1 e^{\tau}) \left\{ \begin{matrix} -\cos\theta \\ \sin\theta \end{matrix} \right\} d\theta \, dz \tag{A-12}$$

A first-order Taylor series expansion of the force components around the steady-state equilibrium position can be written in the form

$$F_r = F_{r0} + Z_{rr}\,\epsilon_1\,e^{\tau} + Z_{rt}\,\epsilon_0\,\varphi_1\,e^{\tau}$$
$$F_t = F_{t0} + Z_{tr}\,\epsilon_1\,e^{\tau} + Z_{tt}\,\epsilon_0\,\varphi_1\,e^{\tau} \tag{A-13}$$

where

$$Z_{ij} = K_{ij} + i\,\nu\,B_{ij}$$
$$i = r,t;\quad j = r,t \tag{A-14}$$

are the bearing impedances. From equations (A-12) and (A-13) the steady-state force components and the impedance coefficients are

$$\left.\begin{matrix} F_{r0} \\ F_{t0} \end{matrix}\right\} = p_a\,R^2 \int_0^{\bar{L}} \int_0^{2\pi} (p_0 - 1) \left\{ \begin{matrix} -\cos\theta \\ \sin\theta \end{matrix} \right\} d\theta\,dz \tag{A-15}$$

$$\left.\begin{matrix} Z_{rr} \\ F_{tr} \end{matrix}\right\} = p_a\,R^2 \int_0^{\bar{L}} \int_0^{2\pi} p_1 \left\{ \begin{matrix} -\cos\theta \\ \sin\theta \end{matrix} \right\} d\theta\,dz \tag{A-16}$$

$$\left.\begin{matrix} Z_{rt} \\ Z_{tt} \end{matrix}\right\} = p_a\,R^2 \int_0^{\bar{L}} \int_0^{2\pi} p_2 \left\{ \begin{matrix} -\cos\theta \\ \sin\theta \end{matrix} \right\} d\theta\,dz \tag{A-17}$$

The steady-state force is

$$F = \sqrt{F_{r0}^{\,2} + F_{t0}^{\,2}};\quad W = -F \tag{A-18}$$

where F is the load capacity of the bearing and W is the bearing load. The angle between the force F and the centerline axis is defined by the equation

$$\phi = \tan^{-1} \frac{F_{r0}}{F_{t0}} \tag{A-19}$$

Under dynamic conditions, the journal (shaft) center whirls in an orbit around its static equilibrium position. The corresponding dynamic bearing reaction is actually a nonlinear function of the amplitude and depends implicitly on time. In a thorough analysis it is necessary to consider the rotor and the bearing simultaneously as was done, for example, in the reference 12. In most practical situations, the amplitude of the shaft motion is, of necessity, rather small. In these cases a linearization of the bearing

reaction is permissible (ref. 5). Then it becomes possible to treat the bearing separately and to represent the bearing reaction by means of coefficients:

$$\begin{aligned} F_x &= - K_{xx}x - B_{xx}\frac{dx}{dt} - K_{xy}y - B_{xy}\frac{dy}{dt} \\ F_y &= - K_{yx}x - B_{yx}\frac{dx}{dt} - K_{yy}y - B_{yy}\frac{dy}{dt} \end{aligned} \tag{A-20}$$

Equation (A-20) is only valid when the journal motion is harmonic, and when

$$\begin{aligned} x &= \bar{x}\, e^{i\nu t} = \bar{x}\, e^{\tau} \\ y &= \bar{y}\, e^{i\nu t} = \bar{y}\, e^{\tau} \end{aligned} \tag{A-21}$$

The equation (A-20) can be written in complex form as

$$\begin{aligned} F_x &= - Z_{xx}x - Z_{xy}y \\ F_y &= - Z_{yx}x - Z_{yy}y \end{aligned} \tag{A-22}$$

where

$$\begin{aligned} Z_{ij} &= K_{ij} + i\ \nu\ B_{ij} \\ i &= x,y;\ \ j = x,y \end{aligned} \tag{A-23}$$

For a given bearing geometry the dynamic coefficients apply to a given static load on the bearing and a given rotor speed. The dynamic coefficients also depend on the whirl frequency, and they are actually impedances of the gas film.

Note that the x-axis was chosen along the direction of the steady-state load. In this case, the dynamic coefficients related to the x-y axis (fig. 1) can be calculated with the equations

$$\begin{aligned} C\ K_{xx} &= (K_{rr}\cos\phi + K_{tr}\sin\phi)\cos\phi - (K_{rt}\cos\phi + K_{tt}\sin\phi)\sin\phi \\ C\ K_{xy} &= (K_{rr}\cos\phi + K_{tr}\sin\phi)\sin\phi + (K_{rt}\cos\phi + K_{tt}\sin\phi)\cos\phi \\ C\ K_{yx} &= (K_{rr}\sin\phi - K_{tr}\cos\phi)\cos\phi - (K_{rt}\sin\phi - K_{tt}\cos\phi)\sin\phi \\ C\ K_{yy} &= (K_{rr}\sin\phi - K_{tr}\cos\phi)\sin\phi + (K_{rt}\sin\phi - K_{tt}\cos\phi)\cos\phi \end{aligned} \tag{A-24}$$

Three parameters are required to specify the coefficients. The most common rotor calculations, other than those for stability investigations, are for critical speeds and unbalanced response. For those conditions the journal whirls synchronously with the rotation such that the whirl frequency equals the rotating frequency.

$$\frac{C\ B_{xx}}{1/\nu} = (B_{rr}\cos\phi + B_{tr}\sin\phi)\cos\phi - (B_{rt}\cos\phi + B_{tt}\sin\phi)\sin\phi$$

$$\frac{C\ B_{xy}}{1/\nu} = (B_{rr}\cos\phi + B_{tr}\sin\phi)\sin\phi + (B_{rt}\cos\phi + B_{tt}\sin\phi)\cos\phi$$

$$\frac{C\ B_{yx}}{1/\nu} = (B_{rr}\sin\phi - B_{tr}\cos\phi)\cos\phi - (B_{rt}\sin\phi - B_{tt}\cos\phi)\sin\phi \qquad \text{(A-50)}$$

$$\frac{C\ B_{yy}}{1/\nu} = (B_{rr}\sin\phi - B_{tr}\cos\phi)\sin\phi + (B_{rt}\sin\phi - B_{tt}\cos\phi\ )\cos\phi$$

In a stability calculation, it is necessary to evaluate the bearing coefficients over a frequency range, usually around one half of the rotating frequency. On the basis of these values, a stability analysis can be performed. If M is the rotor mass supported by the bearing (M = 1/2 of the rotor mass when the rotor is symmetric and rigid) and the bearing is represented by its four Z impedance coefficients, the motion equation can be written as

$$\begin{bmatrix} (Z_{xx} - M\ \nu^2) & Z_{xy} \\ Z_{yx} & (Z_{yy} - M\ \nu^2) \end{bmatrix} \begin{bmatrix} x \\ y \end{bmatrix} = 0 \qquad \text{(A-26)}$$

The threshold of instability occurs when the determinant of the matrix is zero. Noting that

$$Z = K_c + i\nu B_c, \quad K_c = M\ \nu^2 \qquad \text{(A-27)}$$

we can solve the determinant equation to get

$$Z = \frac{1}{2}(Z_{xx} + Z_{yy}) - \sqrt{\frac{1}{4}(Z_{xx} - Z_{yy})^2 + Z_{xy}\ Z_{yx}} \qquad \text{(A-28)}$$

(For stability calculations only the solution with a negative sign in front of the square root proves to be of interest (ref. 5).) At the threshold of instability, Z must be real. The imaginary part of Z can be evaluated over a range of frequencies to find that frequency value ν_0 at which the imaginary part of Z is zero. The corresponding mass is the mass required to make the bearing unstable under the selected working conditions and is

$$M_c = \frac{K_{c0}}{\nu_0^2} \qquad \text{(A-29)}$$

APPENDIX B—HYBRID GAS JOURNAL BEARING ANALYSIS

The geometry and notation for a double-plane, externally pressurized journal bearing is shown in figure 12. The Reynolds equation for steady-state condition of a gas journal bearing becomes

$$\frac{\partial}{\partial\theta}\left(\frac{h^3}{\mu}\rho\frac{\partial p}{\partial\theta}\right) + R^3\frac{\partial}{\partial z}\left(\frac{h^3}{\mu}\rho\frac{\partial p}{\partial z}\right) = 6R^2\Omega\frac{\partial(\rho h)}{\partial\theta} \tag{B-1}$$

Supposing an isothermal evolution of the gas such that

$$\frac{p}{\rho} = \text{constant} \tag{B-2}$$

and using the new natural linearization variable

$$Q = (ph)^2 \tag{B-3}$$

equation (B-1) may be written as

$$\begin{aligned}\frac{\partial^2 Q^{(n+1)}}{\partial\theta^2} + \frac{\partial^2 Q^{(n+1)}}{\partial z^2} - \left(\frac{1}{h}\frac{\partial h}{\partial\theta} + \frac{\Lambda}{h}\frac{1}{\sqrt{Q^{(n)}}}\right)\frac{\partial Q^{(n+1)}}{\partial\theta} \\ - \left(\frac{2}{h}\frac{\partial^2 h}{\partial\theta^2} - \frac{\Lambda}{2h}\frac{1}{\left(Q^{(n)}\right)^{3/2}}\frac{\partial Q^{(n)}}{\partial\theta}\right)Q^{(n+1)} = \frac{\Lambda}{2h}\frac{1}{\sqrt{Q^{(n)}}}\frac{\partial Q^{(n)}}{\partial\theta}\end{aligned} \tag{B-4}$$

where the bearing number is

$$\Lambda = \frac{6\mu\Omega}{p_a}\left(\frac{R}{C}\right)^2 \tag{B-5}$$

Equation (B-4) is written for two successive iterations. To improve the convergence due to the nonlinear terms of the compressible Reynolds equation, a Newton-Raphson method

$$f^{(n+1)}\left(Q,\frac{\partial Q}{\partial x}\right) = f^{(n)}\left(Q,\frac{\partial Q}{\partial x}\right) + \left(\frac{\partial f}{\partial Q}\right)^{(n)}\Delta Q + \left(\frac{\partial f}{\partial\left(\frac{\partial Q}{\partial x}\right)}\right)^{(n)}\Delta\left(\frac{\partial Q}{\partial x}\right) \tag{B-6}$$

is used to write equation (B-4).

Equation (B-4) is valid for all points covering a bearing grid except the edges and the fluid supply points. For a pocketed orifice restrictor supply system (fig. 13), the flow through the supply restrictor and through the film has to be balanced to calculate the pressure downstream of the supply restrictor:

$$\oint_{C_m} \left(\Lambda ph\, \bar{i}_1 - Rh^3 p\, \nabla p \right) \bar{n}\, d\bar{l} = q_m \tag{B-7}$$

The left side of the equation (B-7) represents the flow through the film. For computational convenience the supply hole geometry is slightly modified as shown in figure 14. The right side of the equation (B-7) is the flow through the supply orifice restrictor:

$$q_m = \frac{2\pi \Lambda_s p_s^2}{n} \sqrt{\frac{1+\delta^2}{h_m^2+\delta^2}}\, h_m G_m \tag{B-8}$$

where the restrictor coefficient is

$$\Lambda_s = \frac{6\mu n_0 a^2}{p_s C^3} \sqrt{\frac{\Re T}{1+\delta^2}} \tag{B-9}$$

and

$$\delta = \frac{a^2}{d\, C} \tag{B-10}$$

$$G_m = C_D \begin{cases} \gamma^{\frac{1}{2}} \left(\frac{2}{\gamma+1}\right)^{\frac{\gamma+1}{2(\gamma-1)}} & \text{if } \frac{p_m}{p_s} \le \left(\frac{2}{\gamma+1}\right)^{\frac{\gamma}{\gamma-1}} \\ \left\{ \frac{2\gamma}{\gamma-1} \left(\frac{p_m}{p_s}\right)^{\frac{2}{\gamma}} \left[1 - \left(\frac{p_m}{p_s}\right)^{\frac{\gamma-1}{\gamma}} \right] \right\}^{\frac{1}{2}} & \text{if } \left(\frac{2}{\gamma+1}\right)^{\frac{\gamma}{\gamma+1}} < \frac{p_m}{p_s} \le 1 \\ -\left\{ \frac{2\gamma}{\gamma-1} \left(\frac{p_s}{p_m}\right)^{\frac{2}{\gamma}} \left[1 - \left(\frac{p_s}{p_m}\right)^{\frac{\gamma-1}{\gamma}} \right] \right\}^{\frac{1}{2}} & \text{if } \frac{p_m}{p_s} > 1 \end{cases} \tag{B-11}$$

$$C_D = 1 \qquad \text{if } \frac{p_m}{p_s} \leq \left(\frac{2}{\gamma + 1}\right)^{\gamma-1}$$

$$C_D = 1.155 - 0.555 \left(\frac{p_m}{p_s}\right)^2 \quad \text{if} \frac{p_m}{p_s} > \left(\frac{2}{\gamma + 1}\right)^{\frac{\gamma}{\gamma-1}} \tag{B-12}$$

The discharge coefficient C_D (B-12) was established taking into account data from references 4 and 10.

Note that p_m is the pressure downstream of the supply system and p_s is the supply pressure. Having a first-guess pressure distribution, the pressure p_m can be calculated with equation (B-7) and used like a boundary condition for equation (B-4) in the next iteration.

REFERENCES

1. Castelli, V.; and Pirvics, J.: Review of Numerical Methods in Gas Bearing Film Analysis. J. Lub. Technol., vol. 90, Oct. 1968, pp. 777-792.
2. Booy, M.L.: A Noniterative Numerical Solution of Poisson's and Laplace's Equations with Application to a Slow Viscous Flow. J. Basic Eng., vol. 88, no. 4, Dec. 1966, pp. 725-733.
3. Coleman, R.: The Numerical Solution of Linear Elliptic Equations. J. Lub. Technol., vol. 90, Oct. 1968, pp. 773-776.
4. Gross, W.A.: Fluid Film Lubrication. Wiley, 1980.
5. Lund, J. W.: Calculation of Stiffness and Damping Properties of Gas Bearings. J. Lub. Technol., vol. 90, Oct. 1968, pp. 793-803.
6. Vijayaraghavan, D.; and Keith, T.G., Jr.: An Efficient, Robust and Time Accurate Numerical Scheme Applied to a Cavitation Algorithm. J. Tribol., vol. 112, Jan. 1990, pp. 44-51.
7. Chapra, S.C.; and Canale, R.P.: Numerical Methods for Engineers. Second ed., McGraw-Hill, 1988, Ch. 23, pp. 715-732.
8. Raimondi, A.A.: A Numerical Solution for the Gas-Lubricated Full Journal Bearing of Finite Length. Trans. ASLE, vol. 4, 1961, pp. 131-155.
9. Chang, H.S.; and Pan, C.H.T.: Stability Analysis of Gas-Lubricated, Self-Acting, Plain, Cylindrical, Journal Bearings of Finite Length Using Galerkin's Method. J. Basic Eng., vol. 87, Ser. D, no. 1, Mar. 1965, pp. 185-192.
10. Pink, E.G.: An Experimental Investigation of Externally Pressurized Gas Journal Bearings and Comparison with Design Method Predictions. Proc. 7th Intern. Gas Bearing Symp., Churchill College, Cambridge, England, July 13-15, 1976, pp. G3-41 to G3-59.
11. Wilcock, D.F., ed.: Gas Bearing Design Manual. Mechanical Technology, Inc., Latham, New York, 1972.
12. Castelli, V.; and McCabe, J.T.: Transient Dynamics of a Tilting Pad Gas Bearing System. J. Lub. Technol., Ser. F, vol. 89, no. 4, Oct. 1967, pp. 499-509.

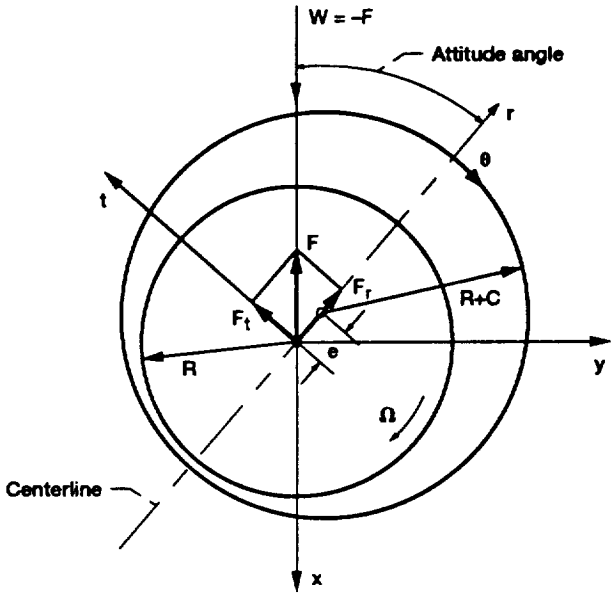

Figure 1.—Journal bearing geometry and notation.

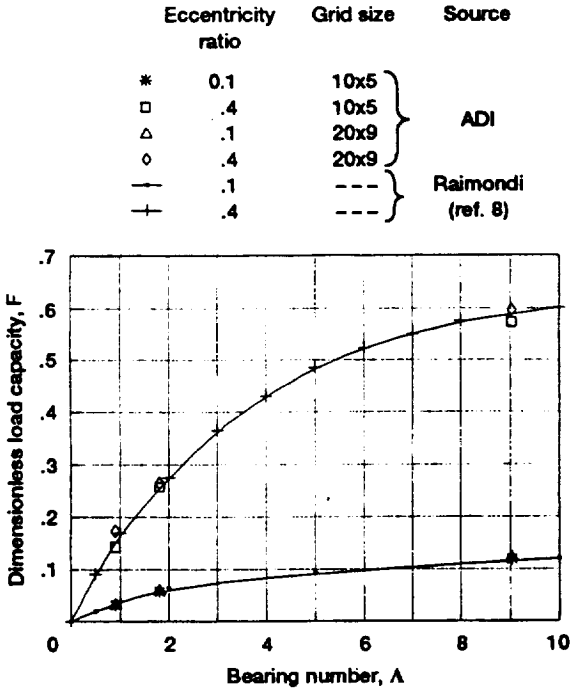

Figure 2.—Aerodynamic journal bearing dimensionless load versus bearing number. ADI method results.

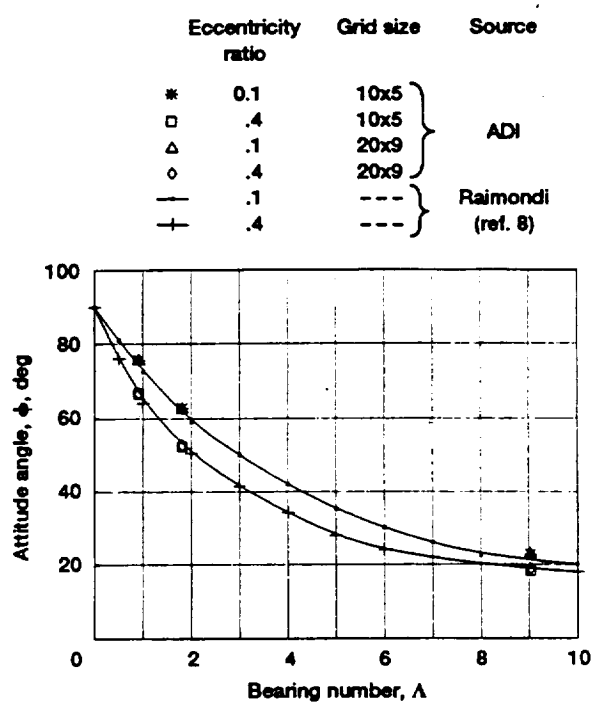

Figure 3.—Aerodynamic journal bearing attitude angle versus bearing number. ADI method results.

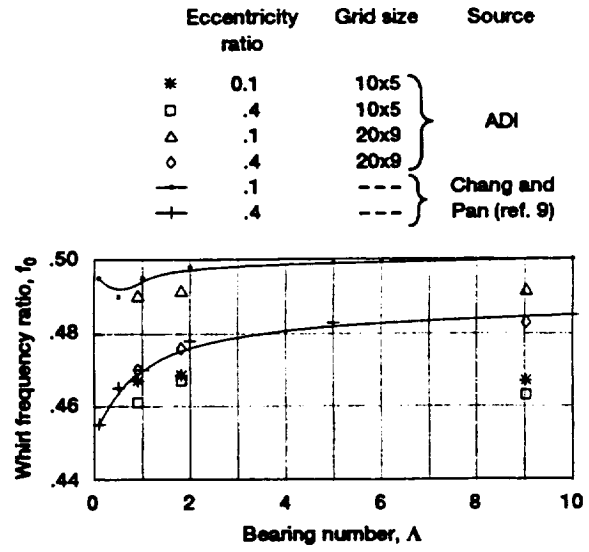

Figure 4.—Aerodynamic journal bearing whirl frequency ratio versus bearing number. ADI method results.

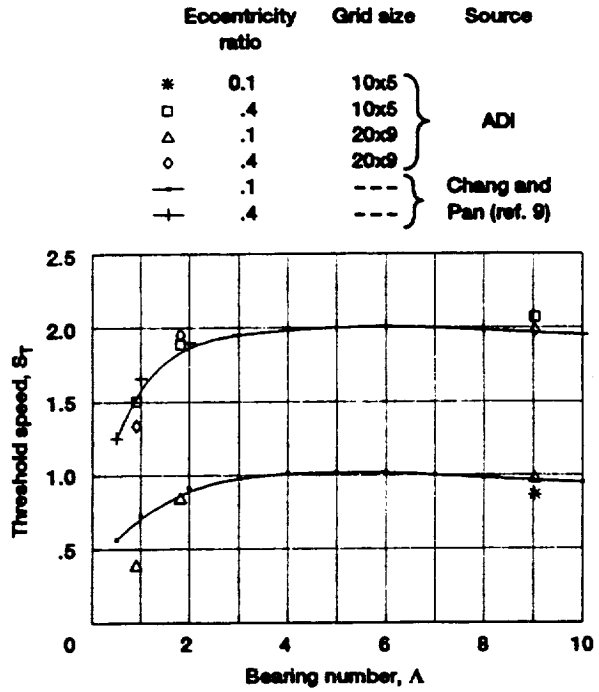

Figure 5.—Aerodynamic journal bearing threshold speed versus bearing number. ADI method results.

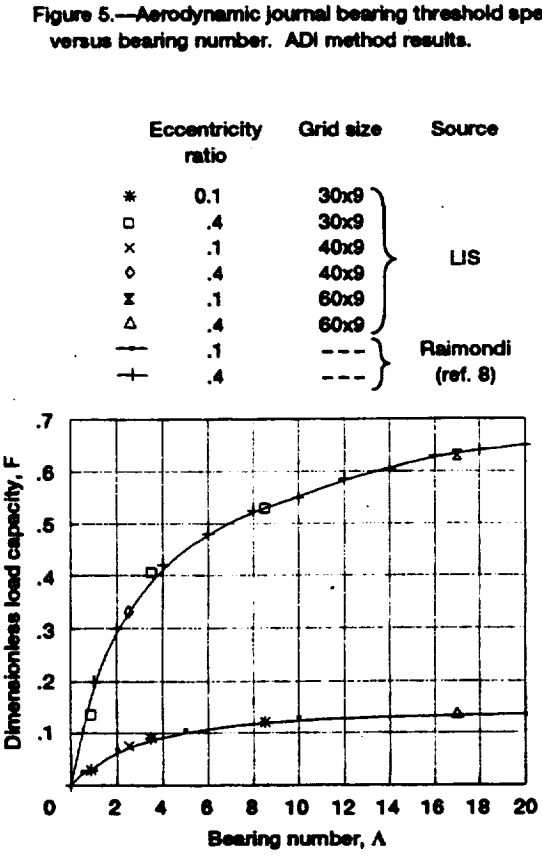

Figure 6.—Aerodynamic journal bearing dimensionless load versus bearing number. LIS data.

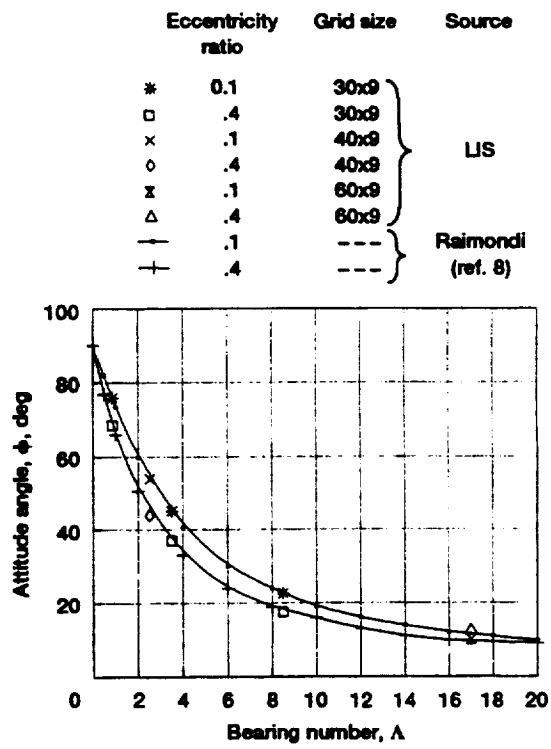

Figure 7.—Aerodynamic journal bearing attitude angle versus bearing number. LIS data.

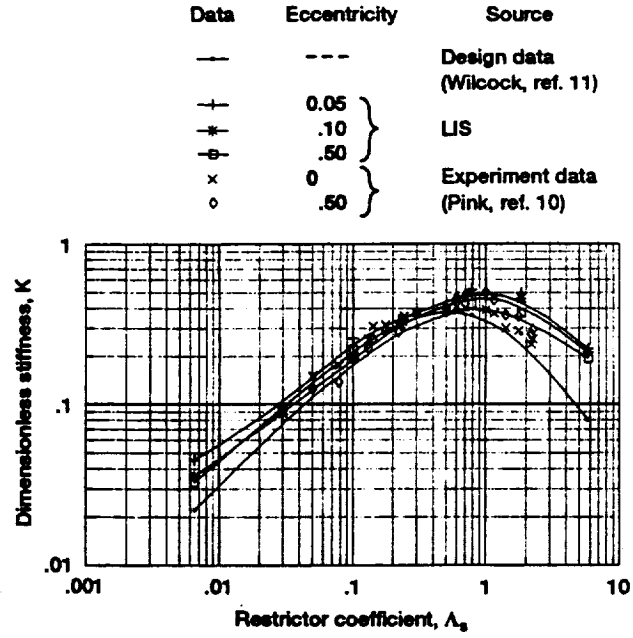

Figure 8.—Comparison of LIS computed stiffness with design data and experimental data. Aerostatic journal bearing; pressure ratio P_s/P_a, 5; length to diameter ratio, L/D, 2; double supply plane; zero speed.

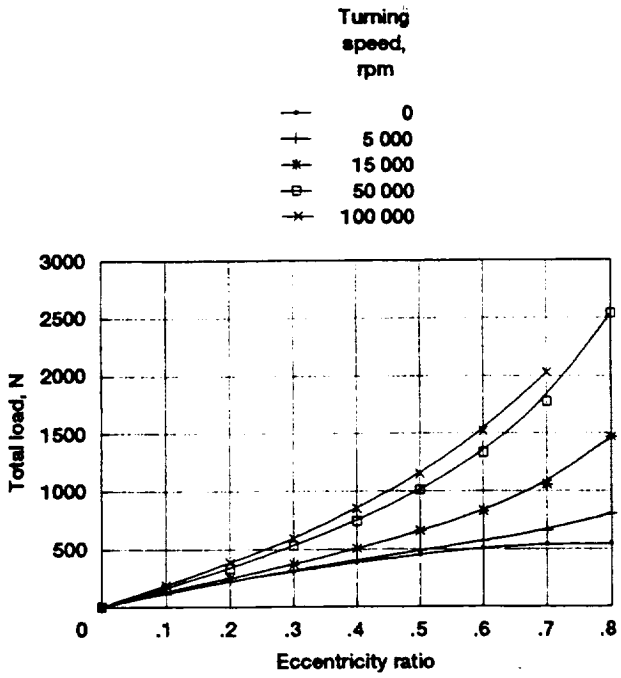

Figure 9.—Total load versus eccentricity ratio as function of turning speed. Hybrid air bearing; length, L, 100 mm; diameter, D, 50 mm; radial clearance, C, 0.02 mm; double supply plane; supply pressure, p_s, 0.5 MPa.

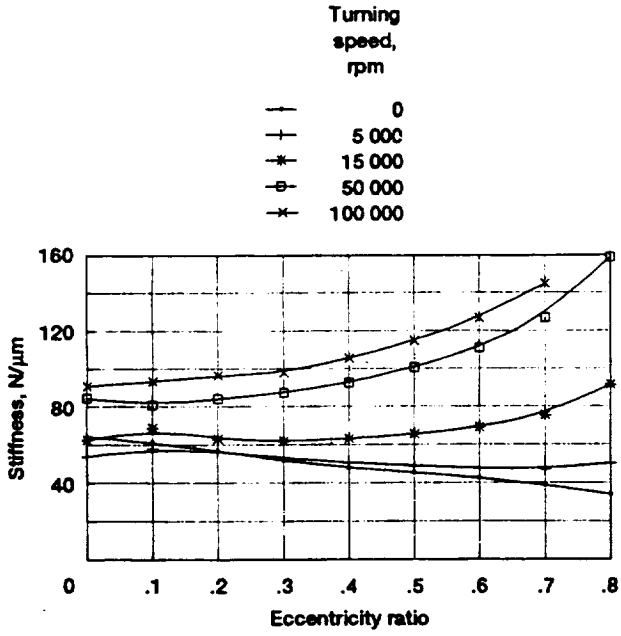

Figure 10.—Stiffness versus eccentricity ratio as function of turning speeds. Hybrid air bearing; length, L, 100 mm; diameter, D, 50 mm; radial clearance, C, 0.02 mm; double supply plane; supply pressure, p_s, 0.5 MPa.

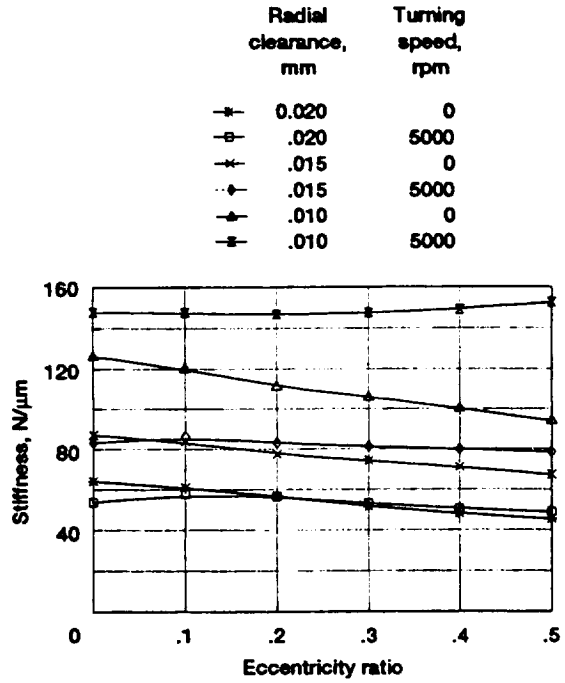

Figure 11.—Stiffness versus eccentricity ratio as function of radial clearance at two turning speeds. Hybrid journal bearing; length, L, 100 mm; diameter, D, 50 mm; double supply plane; supply pressure, p_s, 0.05 MPa.

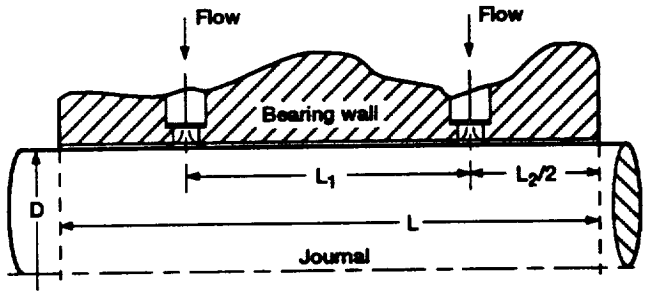

Figure 12.—Externally pressurized gas journal bearing geometry and notation.

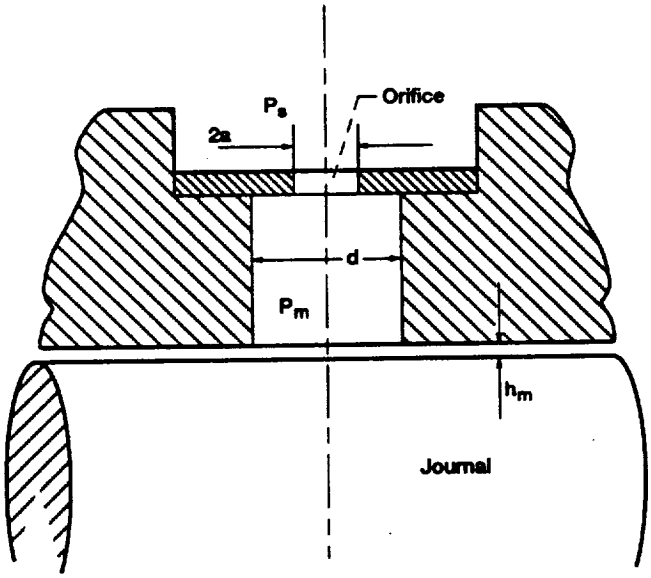

Figure 13.—Supply orifice zone geometry and notation.

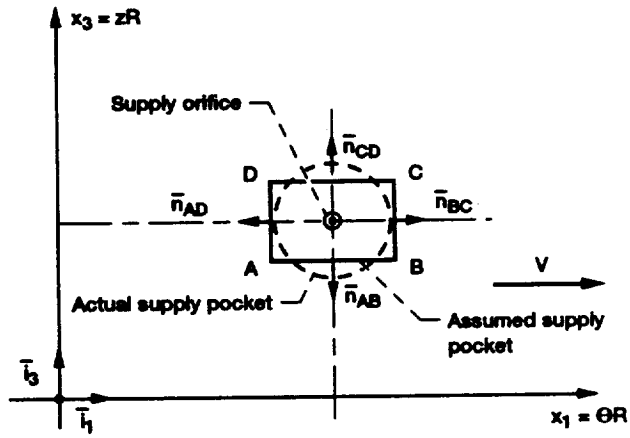

Figure 14.—Supply orifice pocket, analysis assumption.

REPORT DOCUMENTATION PAGE

Form Approved
OMB No. 0704-0188

1. AGENCY USE ONLY (*Leave blank*)	2. REPORT DATE	3. REPORT TYPE AND DATES COVERED
	1992	Technical Memorandum

4. TITLE AND SUBTITLE

Fast Methods to Numerically Integrate the Reynolds Equation for Gas Fluid Films

5. FUNDING NUMBERS

WU-590-21-11

6. AUTHOR(S)

Florin Dimofte

7. PERFORMING ORGANIZATION NAME(S) AND ADDRESS(ES)

National Aeronautics and Space Administration
Lewis Research Center
Cleveland, Ohio 44135-3191

8. PERFORMING ORGANIZATION REPORT NUMBER

E-6824

9. SPONSORING/MONITORING AGENCY NAMES(S) AND ADDRESS(ES)

National Aeronautics and Space Administration
Washington, D.C. 20546-0001

10. SPONSORING/MONITORING AGENCY REPORT NUMBER

NASA TM-105415

11. SUPPLEMENTARY NOTES

Prepared for presentation at the STLE-ASME Joint Tribology Conference, St. Louis, Missouri, October 13-16, 1991. Florin Dimofte, National Research Council-NASA Research Associate at Lewis Research Center. Responsible person, Florin Dimofte, (216) 977-7486.

12a. DISTRIBUTION/AVAILABILITY STATEMENT

Unclassified - Unlimited
Subject Category 37

12b. DISTRIBUTION CODE

13. ABSTRACT (*Maximum 200 words*)

The alternating direction implicit (ADI) method is adopted, modified, and applied to the Reynolds equation for thin, gas fluid films. An efficient code is developed to predict both the steady-state and dynamic performance of an aerodynamic journal bearing. An alternative approach is shown for hybrid journal gas bearings by using Liebmann's iterative solution (LIS) for elliptic partial differential equations. The results are compared with known design criteria from experimental data. The developed methods show good accuracy and very short computer running time in comparison with methods based on an inverting of a matrix. The computer codes need a small amount of memory and can be run on either personal computers or on mainframe systems.

14. SUBJECT TERMS

Tribology; Reynolds equation; Gas fluid film; Hybrid gas journal bearing; Aerodynamic gas journal bearing; Alternating direction implicit method; Liebmann's iterative solution

15. NUMBER OF PAGES

26

16. PRICE CODE

A03

17. SECURITY CLASSIFICATION OF REPORT	18. SECURITY CLASSIFICATION OF THIS PAGE	19. SECURITY CLASSIFICATION OF ABSTRACT	20. LIMITATION OF ABSTRACT
Unclassified	Unclassified	Unclassified	